Cavity Enhancement of Anti-Stokes Scattering via Optomechanical Coupling with Surface Acoustic Waves

Ayato Okada,[1,*] Fumikazu Oguro,[1] Atsushi Noguchi,[1,2] Yutaka Tabuchi,[1] Rekishu Yamazaki,[1,2] Koji Usami,[1] and Yasunobu Nakamura[1,3]

[1]*Research Center for Advanced Science and Technology (RCAST), The University of Tokyo, Meguro-ku, Tokyo 153-8904, Japan*

[2]*PRESTO, Japan Science and Technology Agency, Kawaguchi-shi, Saitama 332-0012, Japan*

[3]*Center for Emergent Matter Science (CEMS), RIKEN, Wako, Saitama 351-0198, Japan*

(Received 31 May 2017; revised manuscript received 16 April 2018; published 2 August 2018)

We report the development of an electro-optomechanical system based on surface acoustic waves (SAWs), where a piezoelectric material with a large optoelastic susceptibility is used for the coupling of both radiowaves and optical light to the SAW. In the optical domain, we exploit the tensorial nature of the optoelastic effect to show the polarization dependence of the photon-SAW interaction. We demonstrate increased coupling both by a two-dimensional SAW-focusing circuit and by the optical cavity enhancement of the photon-phonon scattering. We evaluate the optomechanical coupling rate of the system and discuss the future direction for the improvement of the coupling strength.

DOI: 10.1103/PhysRevApplied.10.024002

I. INTRODUCTION

Cavity optomechanical systems offer a powerful way to optically manipulate the motion of mechanical oscillators ranging from nanoscale objects, such as nanobeams and microtoroidal resonators, to macroscopic objects such as Fabry-Perot interferometers with suspended mirrors [1]. A prominent example is the laser cooling of the mechanical motion into the quantum ground state, achieved both in the microwave and optical regimes [2,3]. Maturity of these techniques and technologies may make the quantum control of macroscopic objects a reality. It is of fundamental interest to investigate quantum properties of macroscopic mechanical oscillators, such as entanglement and decoherence [4–6]. On the other hand, there is a wide range of optomechanical system applications. The unprecedented precision in the displacement and force sensing using mechanical oscillators has been adopted for ultrasensitive measurements, such as the celebrated gravitational-wave detector [7]. One of the unique features of mechanical oscillators is their capability to couple to a wide range of electromagnetic waves, from radiowaves to optical light. Optomechanical systems are considered one of the promising candidates for a microwave-to-light quantum signal transducer [8–11], which is an essential building block for a long-distant quantum network.

Many of the optomechanical systems utilize a "bulk" mode of a mechanical oscillator, including a drum mode of a thin membrane or a flexural mode of a wire. On the other hand, there is a growing interest in using a surface mode, more specifically, surface acoustic waves (SAWs). SAW is a propagating mechanical mode localized on the surface of a substrate. The SAW can easily be excited and manipulated at radiowave and microwave frequencies through patterned electrodes on a piezoelectric substrate or on a piezoelectric film. A SAW resonator with patterned Bragg mirrors has shown a quality factor (Q factor) reaching 10^6 at cryogenic temperatures [12]. Moreover, a localized SAW mode in a high-quality SAW resonator, as well as in a SAW waveguide, can couple to a wide range of physical systems through the strain on the substrate. Strong couplings with a superconducting qubit as well as a nitrogen vacancy (NV) center are realized [13,14]. Construction of SAW-hybrid quantum systems, including quantum dots and trapped ions, are also investigated theoretically [15]. Coupling of the SAW with various physical systems in the optical domain is also being investigated. There are a number of studies on SAW-based acousto-optic modulators [16–18]. The recent development of extremely high-Q microcavities has revived the investigation of stimulated optical excitation of SAWs [19]. Applications of a propagating SAW as a coherent bus for the bulk acoustic resonator [20] and as a modulator for the nanophotonic optical cavity are reported [21–23].

In this paper, we present an optomechanical system, where a SAW resonator is inserted perpendicularly to the light mode of an optical Fabry-Perot cavity. Similar to the "membrane in the middle"-type optomechanical system

*okada@qc.rcast.u-tokyo.ac.jp

[24], the optoelastic effect induced by the strain in the SAW resonator effectively alters the cavity length [25,26]. The focusing effect in the two-dimensional (2D) SAW resonator also enhances the optomechanical coupling. This configuration additionally opens up a utility of the polarization degree of freedom in the optomechanical system, naturally introduced by the anisotropy of the SAW substrate and the tensorial nature of the optoelastic coupling.

II. EXPERIMENT

A. Fabrication and rf spectroscopy of SAW resonators

We fabricate 2D SAW resonators on $LiNbO_3$ substrates with two different cuts, Y-cut and 128° Y-cut, with thicknesses of 500 and 1000 μm, respectively. The substrates are covered with antireflective (AR) coating on both sides. The AR coating is a single-layer SiO_2 with thickness of 183 nm, much smaller than the SAW wavelength of tens of microns, chosen to mitigate the effect on the SAW properties. The SAW resonator circuits are fabricated with photolithography and subsequent wet-etching processes. 100-nm-thick aluminum is evaporated on one side of the substrate and is patterned to form concentric interdigitated transducers (IDTs) and Bragg mirrors. Due to the crystal anisotropy, the group velocity of the SAW strongly depends on the propagating direction. We construct anisotropic IDTs and Bragg mirrors whose contours are proportional to the angular dependence of the group velocity for each crystal to focus the SAW at the center of the SAW resonator [27,28]. The correct contour for the focusing circuits, the IDTs, and the Bragg mirrors, are calculated following the procedure in Ref. [28], which is briefly summarized below. First, the angular-dependent phase velocity of the SAW, $v_p(\theta)$, where θ indicates the angle between the phase-velocity vector of the SAW and the X axis of the crystal, is numerically calculated by solving the Christoffel equation with a semi-infinite boundary condition with material constants provided in Ref. [29]. From the calculated $v_p(\theta)$, the angular distribution of the group velocity $v_g(\phi)$ can be obtained using the relations

$$v_g = v_p \left[1 + \left(\frac{1}{v_p} \frac{dv_p}{d\theta} \right)^2 \right]^{1/2} \tag{1}$$

$$\phi = \theta + \arctan\left(\frac{1}{v_p} \frac{dv_p}{d\theta} \right), \tag{2}$$

where ϕ indicates the angle between the group-velocity vector of the SAW and the X axis of the crystal. One can also determine the anisotropic piezo coupling strength from the calculated phase velocities for the metalized and the free surface [30]. For the construction of IDTs and Bragg mirrors, we simply plot and scale the group-velocity contour, $v_g(\phi)$, calculated above. Computer aided design images of the sample are shown in Figs. 1(a) and 1(b). In all samples, both the width and the spacing of the electrodes in the IDTs and the Bragg mirrors are 10 μm, which excites the SAW with a wavelength of $\lambda_{SAW} \simeq 40$ μm. For this width, the Y-cut and 128° Y-cut SAW resonators are expected to have resonance frequencies of 87.2 and 99.9 MHz, with corresponding SAW velocities of 3488 and 3997 m/s, respectively [30]. The samples are fixed with varnish on a sample holder and the IDT ports are wire bonded to SMA connectors, as shown in Fig. 1(c).

We conduct radiofrequency (rf) transmission measurement (S_{21} measurement) on the samples using a vector network analyzer. The S_{21} measurement is performed through an IDT with port 1 being the top electrode of the IDT in Fig. 1(a) and port 2 being the bottom electrode of the same IDT. The measurement result shows an interference of the direct transmission of the rf signal through the capacitive coupling between the two IDT electrodes with the signal mediated by the SAW resonator. The total impedance of the circuit is decomposed into two parts, an electric impedance owing to the capacitance between the IDT fingers and an acoustic impedance owing to the acoustic wave generation. Our measurement scheme is sufficient to characterize the SAW resonator because the acoustic impedance of the circuit rapidly changes near the acoustic resonance through the conversion of the electrical signal to the SAW. The resonance frequency of the SAW resonator appears as the peak on a broad background, as shown in Fig. 1(d). By fitting the spectroscopic data, we find the SAW resonances at 86.4 and 98.3 MHz, with corresponding Q factors of $Q \simeq 50$ and 450, for Y-cut and 128° Y-cut $LiNbO_3$ samples, respectively. The low-Q factors of these samples are presumably due to the anisotropy of the SAW propagation and the small misalignment of the Bragg mirror structure with respect to the crystal axis in the fabrication process. For a comparison, in one-dimensional Fabry-Perot SAW resonators, we repeatedly obtain $Q \sim 10^4$ using the same fabrication condition. The particularly low-Q factor observed in the Y-cut sample is presumably due to the combination of the contour imperfection and the relatively isotropic piezo coupling. Due to the contour imperfection, the SAW propagating toward a different angle has a slightly different resonance frequency. When the material has piezo coupling at all angles, these different resonances are excited simultaneously, resulting in the "inhomogeneous broadening" of the resonator.

B. Sideband scattering due to optoelastic effect and SAW focusing

Next we perform an optical measurement (Fig. 2), where the phase shift of the probe beam induced by the optoelastic effect in the SAW resonator is detected through a heterodyne detection. The probe laser light at a wavelength of $\lambda_{opt} = 1064$ nm is tightly focused near the center of the

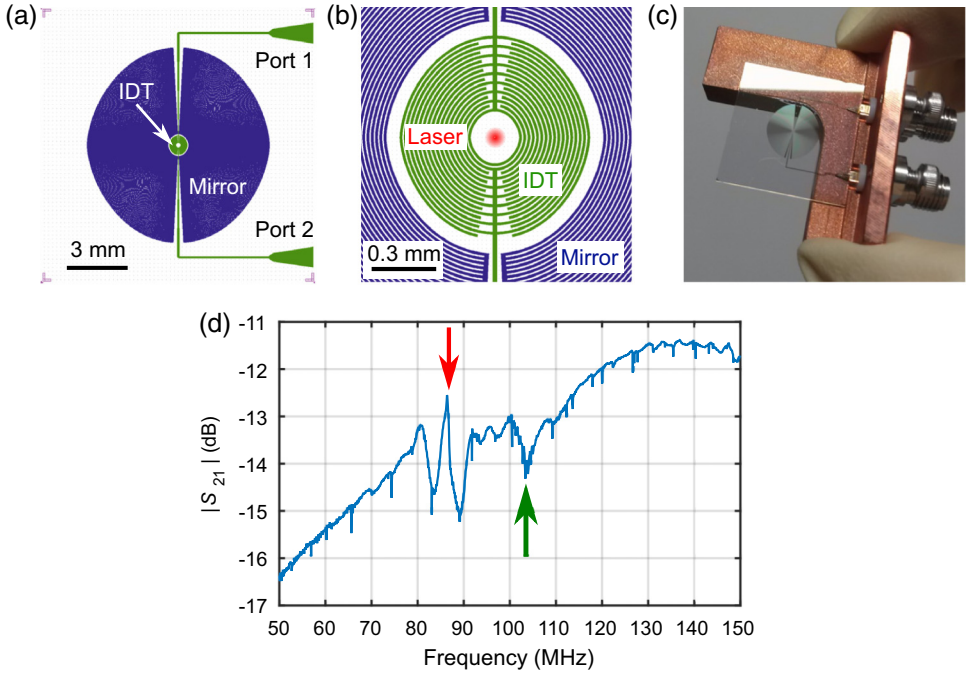

FIG. 1. Two-dimensional SAW resonator. (a) Design of the SAW-focusing circuit. The outer (blue) and inner (green) patterns form a concentric Bragg mirror and an interdigitated transducer (IDT), respectively. (b) Magnified view of the center part. The width and spacing of the electrodes are 10 μm. In order to map out the spatial variation of the optoelastic effect, a laser beam is scanned across the central region free from electrodes. (c) Photograph of a SAW resonator. Aluminum electrodes are evaporated on Y- and 128° Y-cut $LiNbO_3$ substrates. The chip is mounted on a sample holder and wire bonded to the SMA connectors. (d) Radio-frequency transmission spectrum from port 1 to port 2 through the SAW resonator. A clear SAW resonance peak is observed at 87 MHz (red arrow) with a linewidth of 1.7 MHz. A dip around 105 MHz is attributed to a leaky SAW mode (green arrow). Other spurious spikes are the overtones of the longitudinal and shear modes of the bulk waves. All the materials shown in (a)–(d) are of the Y-cut sample.

SAW resonator. The rf voltage excites the SAW resonator mode, and the optoelastic phase modulation imparted by the SAW produces red and blue sidebands. We use a lock-in detection scheme to obtain the amplitude of the sideband signal. The heterodyne signal between the generated sideband light and the local oscillator beam is detected on a fast photodetector and sent to a lock-in amplifier (Zurich Instruments HF2LI), which enables the evaluation of only one of the sidebands. Previously, a similar heterodyne detection experiment was performed to map out a spatial profile of a bulk acoustic wave (BAW) resonator [31]. This measurement exploited the reflected optical signal from the metalized surface of the BAW resonator to measure the surface displacement. In our detection scheme, where we measure the transmission signal, the signal is susceptible to the elongation (and contraction) of the material, which results from the surface displacement, as well as the strain-induced change of the refractive index. The variation of the refractive index effectively changes the material thickness. The latter effect is found to be dominant in our experiment as we later show.

The sample is scanned along the *XZ* plane perpendicular to the propagation direction of the laser light. The result of the 2D mapping is shown in Fig. 3(a), where the

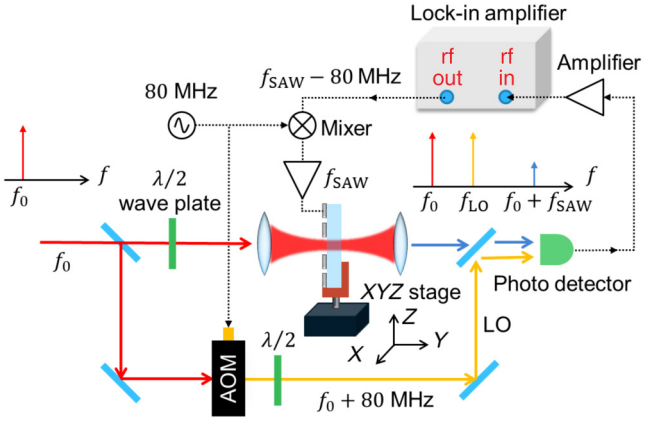

FIG. 2. Experimental setup for probing the optical modulation imparted by the SAW-induced optoelastic effect. A rf signal at around 87 MHz is applied to the device for the SAW excitation. A focused laser beam is sent through the SAW device. The heterodyne signal with a local oscillator (LO) laser is detected and demodulated with a lock-in amplifier to observe the phase modulation. The laser beam width at the SAW device is estimated to be 3.5 μm, much smaller than the SAW wavelength of 40 μm. The SAW device is attached to an *XYZ*-stage, which allows observation of the spatial distribution of the phase modulation.

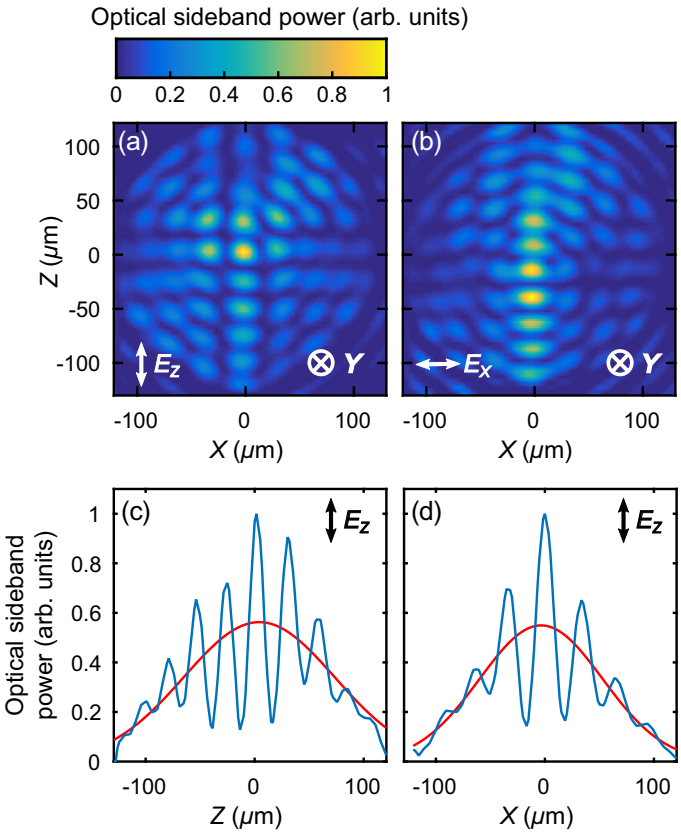

FIG. 3. Upper panel: Spatial distribution of the laser phase modulation imparted by the SAW on the Y-cut $LiNbO_3$ sample. Color maps show the normalized power of the generated sideband signal for the input laser of (a) Z and (b) X polarizations, respectively. Coordinates are aligned to the crystal axes of the sample. Lower panel: Cross sections (blue) attained by summing up the signal in (a) along the (c) X and (d) Z direction. Gaussian fitting (red) to the data yields effective radii of (c) $R_Z = 100\ \mu$m and (d) $R_X = 80\ \mu$m as the $1/e$ decay length of the fitted Gaussian.

polarization of the laser beam is parallel to the Z direction. We note that the coordinates are aligned with the crystal axes of the $LiNbO_3$ substrate. In the modulation pattern, we observe the focusing of the SAW at the center of the resonator. The observed fringe period reflects the standing wave patterns expected for $\lambda_{SAW} = 40\ \mu$m.

From the tensorial property of the optoelastic effect, one expects different modulation patterns for different input beam polarization. Changing the polarization of the probe beam to the X direction, with the SAW excitation frequency fixed, yields a quite different 2D image, as shown in Fig. 3(b). This observation indicates that the origin of sideband generation is, in fact, due to the optoelastic effect and not the surface displacement. While the standing wave pattern is formed both in the X and Z directions in Fig. 3(a), that of Fig. 3(b) breaks the symmetry and is formed strongly in the Z direction.

We can understand this observation qualitatively by considering the variation of the refractive index due to the optoelastic effect. The optoelastic tensor contains eight independent coefficients p_{11}, p_{12}, p_{13}, p_{14}, p_{31}, p_{33}, p_{41}, and p_{44} in the abbreviated notation [32]. Under the assumption that the Y component of the displacement vector, u_y, is dominant in the optoelastic effect in the present setup, the relevant coefficients are only $p_{12} = 0.088$, $p_{14} = -0.083$, and $p_{31} = 0.177$ [33]. For the Z-polarized light it can be written as

$$\delta n_z = -\frac{1}{2} n_e^3 p_{31} \frac{\partial u_y}{\partial y}, \tag{3}$$

and for the X-polarized light as

$$\delta n_x = -\frac{1}{2} n_o^3 \left(p_{12} \frac{\partial u_y}{\partial y} + p_{14} \frac{\partial u_y}{\partial z} \right), \tag{4}$$

where $n_e = 2.16$ and $n_o = 2.24$ are the refractive indices for the extraordinary and the ordinary light, respectively. Equation (3) only contains the term $\partial u_y/\partial y$, the elongation rate along the Y axis, whose distribution is visualized in Fig. 3(a), and under our assumption it may faithfully represent the SAW distribution in the resonator. On the other hand, Eq. (4) contains the additional term $\partial u_y/\partial z$, which causes the biased distribution toward the Z axis and displaces the location of the maximum phase modulation along the Z axis from $Z = 0$ in Fig. 3(b).

A conventional SAW resonator with a one-dimensional uniform standing wave has a simple mode area A, defined by the extent of the resonator. The SAW-focusing technique in the 2D concentric resonator allows one to reduce the mode area by concentrating the mode intensity at the focus of the resonator. In such resonators, the spatial distribution of the SAW mode amplitude follows Bessel functions. Integrating the mode distribution in the circular area defined by the circuit, the mode has an effective area, $A = \pi R_{\rm eff}^2 J_1^2(\alpha_{0n})$, where $R_{\rm eff}$ is the effective radius of the circuit including a penetration depth into the Bragg mirror, J_1 is the first-order Bessel function, and α_{0n} is the argument of the nth zero of the zeroth-order Bessel function J_0, with $n \sim 2R_{\rm eff}/\lambda_{\rm SAW}$ being a number of nodes contained within the effective radius when n is large. For $R_{\rm eff} \gg \lambda_{\rm SAW}$, the expression simplifies to $A = \eta \lambda_{\rm SAW} R_{\rm eff}$, with $\eta \sim 0.32$. The focusing in two dimensions allows the reduction of the mode area from the form $A = \pi R_{\rm eff}^2$ to $A = \eta \lambda_{\rm SAW} R_{\rm eff}$. Using these expressions along with the effective radius of the original SAW resonator, $R_{\rm eff} \sim 1$ mm, and the wavelength $\lambda_{\rm SAW} = 40\ \mu$m, the mode area is expected to be reduced by a factor of 250. In order to estimate an effective mode area of the 2D SAW resonator, we fit a Gaussian function to the SAW distribution, as shown in Figs. 3(c) and 3(d). The fit yields effective radii; $R_Z = 100\ \mu$m and $R_X = 80\ \mu$m, which are defined as the $1/e$ decay length of the fitted Gaussian. The effective mode area, expressed as

$\pi R_X R_Z$, is approximately 1/100 of the resonator's original mode area. The deviation from the theoretically estimated value indicates the necessity of further optimization in the design and fabrication process of the SAW resonator.

While the focusing effect on the Y-cut sample is apparent, the effect is observed to be relatively weaker for the 128° Y-cut sample. For the 128° Y-cut case, the piezo coupling in the X direction is about six times stronger than the orthogonal direction in the SAW plane. The strong piezo coupling effectively creates a 1D SAW resonator along the X direction, resulting in the weaker focusing pattern. To fully utilize the focusing effect, it is preferable to choose a crystal cut with relatively isotropic piezo coupling in the SAW plane.

C. Polarization-dependent light-SAW coupling

Utilizing the tensorial property derived above, we can selectively couple light to the SAW. For example, for the beam spot focused at a node of the standing SAW mode in Fig. 3(a), the Z-polarized light is weakly modulated by the SAW, yet the X-polarized light is subject to strong modulation due to the second term of Eq. (4). To demonstrate this, we compare the depth of the phase modulation at two different positions, denoted A and B in Fig. 4(a), for different light polarizations. First we set the beam spot at position A in Fig. 4(a) and sweep the rf frequency to obtain the sideband power spectrum for the X- and Z-polarized light, shown as red and blue solid lines in Fig. 4(b), respectively. Next, we move to position B in Fig. 4(a), and perform the same measurement [Fig. 4(c)]. At position A, each polarization is subject to nearly the same amount of modulation imparted by the SAW mode. However, at position B, Z-polarized light is hardly modulated while the X-polarized light still shows a sufficient modulation at the same frequency. Figure 4(d) shows the ratio of the sideband power generated by the X- and Z-polarized light at position B. At the SAW excitation frequency of 86.78 MHz, the modulation of the Z-polarized light is 300 times smaller than that of the X polarization light, showing strong selectivity of light-SAW coupling depending on the polarizations.

D. SAW-in-the-middle optomechanical system

The observed optoelastic effect can be utilized to compose an optomechanical system. We insert the 2D SAW resonator to an optical Fabry-Perot cavity, where the

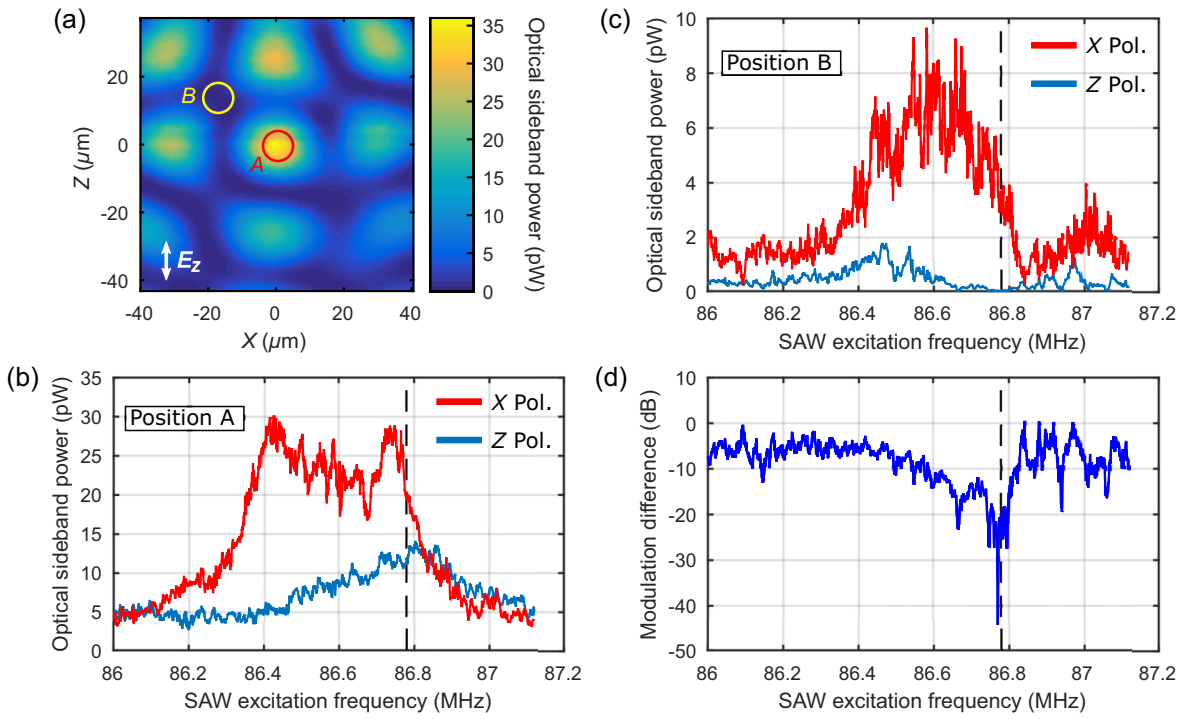

FIG. 4. Polarization dependence of the SAW-induced laser phase modulation. (a) Spatial distribution of the SAW resonator mode near its center, probed with the Z-polarized laser light. Position A, indicated by the red circle, corresponds to the center antinode of the SAW resonator, where the maximum modulation is observed. Position B (yellow circle) is one of the nodes. (b) Power spectra of the sideband generated by the X- (red) and Z- (blue) polarized light at position A. (c) The same spectrum taken at position B. (d) Ratio of the sideband power generated by the X and Z polarization light at position B. The black dashed lines in (b)–(d) indicate the SAW excitation frequency used in (a). All the materials shown in (a)–(d) are of the Y-cut sample. The acoustic excitation power is −5 dBm for (a) and −9.3 dBm for (b)–(d).

coupling between the SAW resonator and the optical cavity field via the optoelastic effect is investigated. The experimental setup is shown in Fig. 5(a). The cavity is composed of two identical mirrors with a reflectivity of approximately 99.5%, and a radius of curvature of 25 mm. A cavity length of about 50 mm, near the concentric configuration, is chosen to tightly focus the beam at the waist. The radius of the beam at the waist is estimated to be 20 μm, below which the optical cavity becomes unstable. The unloaded cavity linewidth is measured to be 3.6 MHz, and we do not observe any measurable deterioration of the cavity finesse after loading the AR-coated SAW resonator chip inside the cavity. The AR coating on the chip is quite important. In our initial attempt without an AR coating, a large reflection of up to 15% from each surface, owing to a large refractive index of $LiNbO_3$, is enough to make the optical cavity unstable.

With the SAW sample inside the optical cavity, we perform optical spectroscopy to observe the cavity-enhanced anti-Stokes scattering by the SAW resonator. The resonance frequency of the optical cavity is stabilized to that of the reference laser (frequency f_c) via the Pound-Drever-Hall technique [34]. While exciting the SAW by applying a rf signal to the IDT, we inject a strong pump power from the opposite side of the reference laser under the detuning condition $\delta = f_c - (f_{\rm pump} + f_{\rm SAW}) \simeq 0$. [See the frequency diagram in Fig. 5(b).] The upper sideband of the pump laser scattered into the optical cavity mode is measured as a heterodyne signal between the up-converted signal and the reference laser reflected from the cavity. The cavity-enhanced scattering is expected to be large near $\delta \simeq 0$. As shown in Fig. 5(c), we observe a Lorentzian-shape resonance, which shows significant enhancement of anti-Stokes scattering when the detuning between f_c and $f_{\rm pump}$ is tuned to the mechanical frequency of the SAW resonator. From the fit to the data, the linewidth of the resonance is determined to be nearly identical to the cavity linewidth independently measured. The observed cavity-enhanced anti-Stokes scattering suggests that the SAW resonator is optomechanically coupled to the optical cavity.

We analyze the system from the viewpoint of cavity optomechanics to evaluate the optomechanical coupling rate and other related parameters experimentally. We focus the laser light at the center of the SAW resonator, while resonantly exciting the SAW by the rf signal with input power $P_{\rm SAW}$. The calibration is performed by single-path transmission of light (without the optical cavity). We first calibrate the phonon number stored in the SAW resonator, $N_{\rm SAW}$, from the rf reflection measurement (S_{11} measurement). Second, we measure the amount of optical phase modulation, $\phi_{\rm SAW}$, imparted by the SAW by comparing the generated sideband power with that of a calibrated electro-optic modulator. The phase modulation imparted by the zero-point fluctuation of the SAW in the resonator, $\phi_{\rm zpf}$, can be estimated as $\phi_{\rm zpf} = \phi_{\rm SAW}/\sqrt{N_{\rm SAW}}$. The

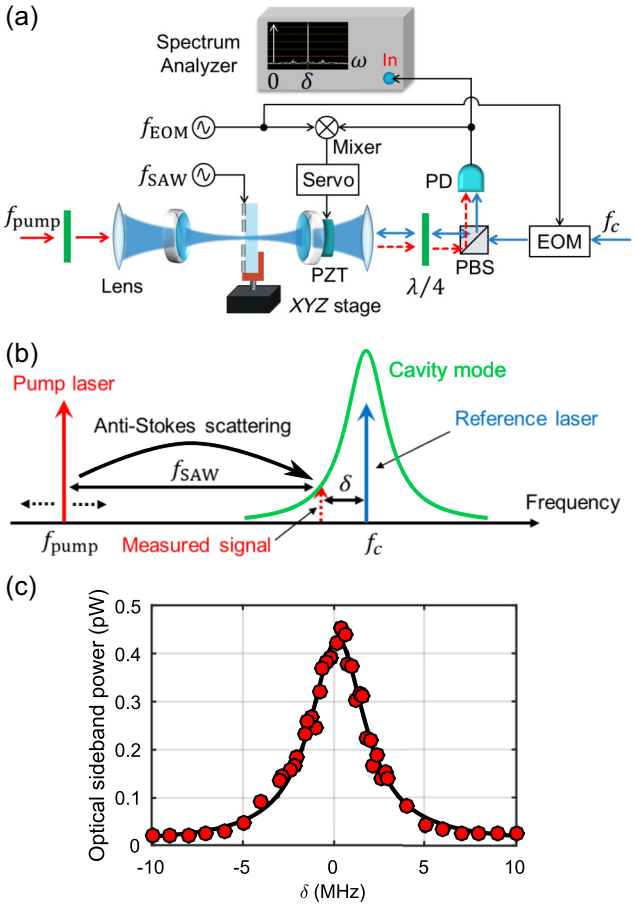

FIG. 5. (a) Experimental setup for the measurement of the cavity-enhanced anti-Stokes scattering. The SAW resonator is inserted at the waist of a Fabry-Perot cavity. A reference laser (blue arrow) is used for the stabilization of the cavity spacing. While exciting the SAW resonator by a rf signal, detuned pump laser (solid red arrow) is injected from the opposite side of the cavity, from which the anti-Stokes scattering is observed (dotted red line). It is detected through the heterodyne measurement using the reference laser reflected back from the cavity. PD, photo detector; PBS, polarizing beamsplitter; PZT, piezoelectric actuator; EOM, electro-optic modulator; $\lambda/4$, quarter-wave plate. (b) Frequency diagram of the measurement. The pump laser frequency is set on the red side of the cavity resonance. Anti-Stokes scattering of the pump laser is enhanced by the optical cavity mode when the detuning δ is close to zero. (c) Cavity-enhanced spectrum. The scattered light power shows a peak when the pump laser is swept across $\delta = 0$. The observed linewidth of 3.6 MHz is consistent with the cavity linewidth measured independently. The result is obtained for the 128° Y-cut $LiNbO_3$ sample. The acoustic excitation power is -5 dBm.

optomechanical coupling rate g_0 is defined as the shift of the cavity resonance frequency induced by a single phonon, $g_0 = (\omega_c/L)\delta x$, where ω_c is the resonance frequency of the optical cavity, L is the cavity length, and δx is the effective variance of the cavity length due to the zero-point motion of the SAW, in our case, written

as $\delta x = (\phi_{\rm zpf}/2\pi)\,\lambda_{\rm opt}$. For the Y-cut substrate, we find an optomechanical coupling rate of $g_0/2\pi = 60$ mHz.

The amplitude of the zero-point motion of the SAW, $u_{\rm zpf}$, can be obtained through dividing u_y by $\sqrt{N_{\rm SAW}}$. The amplitude u_y is inferred from a relationship $\partial u_y/\partial z \simeq k_{\rm SAW}\,u_y$, where $\partial u_y/\partial z$ is the shear strain appearing in Eq. (4) and $k_{\rm SAW}$ represents a wavenumber of the SAW corresponding to $\lambda_{\rm SAW} = 40\ \mu$m. The shear strain can be experimentally derived from Eqs. (3) and (4) by measuring the phase modulations due to the optoelastic effect with each polarization. Measured phase modulations can be written as the variance of the refractive indices, $\phi_{\rm SAW}/2\pi = (\lambda_{\rm SAW}/\lambda_{\rm opt})\delta n$, where we assume that the interaction between the light and the SAW occurs within one wavelength of the SAW due to the geometry of the current experimental setup. We finally find $u_{\rm zpf} = 0.5 \times 10^{-2}$ fm, while a theoretical estimation derived from a value reported in [15], along with the effective mode area of the SAW resonator of $\pi \times 80\ \mu$m $\times$ $100\ \mu$m, yields $u_{\rm zpf} = 1 \times 10^{-2}$ fm. The theoretical value is compatible with the experimentally estimated value, taking into account the large uncertainty around one order of magnitude accompanied by the calibration of $N_{\rm SAW}$.

III. PROSPECTS

We observe an indication of SAW focusing in a 2D resonator and optomechanical coupling between the SAW and the optical cavity. However, the deterioration of the Q factor of the SAW resonator and the small optomechanical coupling rate are serious problems to be tackled. In order to obtain a high-Q factor in the focusing circuit, the SAW material constants, such as elastic and piezoelectric constants, from which we derive the group velocity distribution, need to be determined with high precision. The inaccuracy of the electrode orientation with respect to the crystal axis in the fabrication process can be a deterioration factor as well. In practice, it is not straightforward to achieve an extremely high-Q factor with $LiNbO_3$ or other anisotropic materials. Instead, it is much easier to use a nonpiezoelectric isotropic substrate with a piezoelectric film such as polycrystalline AlN and ZnO, so that simple circular electrodes can be used to achieve the focused SAW mode whose Q factor is limited by the internal loss and not from the velocity dispersion.

The small optomechanical coupling rate is mostly attributed to the large optical cavity mode volume and the small mode overlap between the optical and SAW modes. The optoelastic coupling is inversely proportional to the cavity length, $g_0 \propto 1/L$, where L is the length of the optical cavity. If a commercially available $LiNbO_3$ substrate with a thickness of 100 μm is used along with a fiber-optical cavity construction [35,36] with a cavity length of 300 μm, the optomechanical coupling rate of the order of 10 Hz can be achieved. The system's cooperativity defined by $C = 4ng_0^2/\gamma\kappa$, where n indicates intracavity photon numbers, and κ and γ are decay rates of the optical cavity and the SAW resonator, respectively, will be increased up to $C \simeq 1$ after the modification described above, assuming an optical input power of 10 mW and a mechanical Q factor of 10^5, which we observe in a conventional planar SAW resonator on the $LiNbO_3$ substrate. In this regime, optomechanical control of the SAW resonator mode such as resolved sideband cooling will be possible. In addition, the rigid solid-state SAW device along with the fiber-based cavity will make the system more robust in the cryogenic environment. Operated in the environment at 10 mK, our transducer based on the high-frequency SAW resonator can be cooled near the quantum ground state and will enable a faithful transduction of quantum signals.

For further improvement of the coupling strength, changing the coupling geometry is desirable. An optical waveguide embedded under a planar SAW resonator, where wave vectors of both acoustic and optical waves are parallel, along with an appropriate phase-matching condition, will ideally accomplish the perfect mode overlap between the acoustic and the optical field.

We also observe the unique polarization dependence of the photoelastic coupling. Our device opens up a new avenue in the application of the optomechanical system, where an optical polarization can be used as an additional degree of freedom. In the context of quantum communication, the photon qubit basis which allows the heralded protocols, such as polarization or time-bin basis, are preferred. Applications including polarization-to-Fock-state conversion between the optical and microwave signals may be possible.

IV. CONCLUSION

In conclusion, we demonstrate an enhancement of the optomechanical coupling with a SAW-based optomechanical system. The enhancement is achieved by exploiting the SAW-focusing technique as well as the optical cavity. The unique feature of the optoelastic coupling with polarization dependence is also observed.

ACKNOWLEDGMENTS

The authors acknowledge K. Kusuyama, M. Ataka, and H. Fujita for their help in sample fabrication. This work was partly supported by JSPS KAKENHI (Grant No. 26220601), NICT, JST PRESTO (Grant No. JPMJPR-1429), and JST ERATO (Grant No. JPMJER1601).

[1] M. Aspelmeyer, T. J. Kippenberg, and F. Marquardt, Cavity optomechanics, Rev. Mod. Phys. **86**, 1391 (2014).

[2] J. D. Teufel, T. Donner, D. Li, J. W. Harlow, M. S. Allman, K. Cicak, A. J. Sirois, J. D. Whittaker, K. W. Lehnert, and R. W. Simmonds, Sideband cooling of micromechanical motion to the quantum ground state, Nature (London) **475**, 359 (2011).

[3] J. Chan, T. P. M. Alegre, A. H. Safavi-Naeini, J. T. Hill, A. Krause, S. Gröblacher, M. Aspelmeyer, and O. Painter, Laser cooling of a nanomechanical oscillator into its quantum ground state, Nature (London) **478**, 89 (2011).

[4] S. Bose, K. Jacobs, and P. L. Knight, Preparation of nonclassical states in cavities with a moving mirror, Phys. Rev. A **56**, 4175 (1997).

[5] S. Mancini, V. I. Man'ko, and P. Tombesi, Ponderomotive control of quantum macroscopic coherence, Phys. Rev. A **55**, 3042 (1997).

[6] S. Bose, K. Jacobs, and P. L. Knight, Scheme to probe the decoherence of a macroscopic object, Phys. Rev. A **59**, 3204 (1999).

[7] B. P. Abbott et al. (LIGO Scientific Collaboration and Virgo Collaboration), Observation of Gravitational Waves from a Binary Black Hole Merger, Phys. Rev. Lett. **116**, 061102 (2016).

[8] J. Bochmann, A. Vainsencher, D. D. Awschalom, and A. N. Cleland, Nanomechanical coupling between microwave and optical photons, Nat. Phys. **9**, 712 (2013).

[9] R. W. Andrews, R. W. Peterson, T. P. Purdy, K. Cicak, R. W. Simmonds, C. A. Regal, and K. W. Lehnert, Bidirectional and efficient conversion between microwave and optical light, Nat. Phys. **10**, 321 (2014).

[10] T. Bagci, A. Simonsen, S. Schmid, L. G. Villanueva, E. Zeuthen, J. Appel, J. M. Taylor, A. Sørensen, K. Usami, A. Schliesser, and E. S. Polzik, Optical detection of radio waves through a nanomechanical transducer, Nature (London) **507**, 81 (2014).

[11] R. Hisatomi, A. Osada, Y. Tabuchi, T. Ishikawa, A. Noguchi, R. Yamazaki, K. Usami, and Y. Nakamura, Bidirectional conversion between microwave and light via ferromagnetic magnons, Phys. Rev. B **93**, 174427 (2016).

[12] R. Manenti, M. J. Peterer, A. Nersisyan, E. B. Magnusson, A. Patterson, and P. J. Leek, Surface acoustic wave resonators in the quantum regime, Phys. Rev. B **93**, 041411(R) (2016).

[13] M. V. Gustafsson, T. Aref, A. F. Kockum, M. K. Ekström, G. Johansson, and P. Delsing, Propagating phonons coupled to an artificial atom, Science **346**, 207 (2014).

[14] D. A. Golter, T. Oo, M. Amezcua, K. A. Stewart, and H. Wang, Optomechanical Quantum Control of a Nitrogen-Vacancy Center in Diamond, Phys. Rev. Lett. **116**, 143602 (2016).

[15] M. J. A. Schuetz, E. M. Kessler, G. Giedke, L. M. K. Vandersypen, M. D. Lukin, and J. I. Cirac, Universal Quantum Transducers Based on Surface Acoustic Waves, Phys. Rev. X **5**, 031031 (2015).

[16] S. S. Hong, M. S. Mermelstein, and D. M. Freeman, Reflective acousto-optic modulation with surface acoustic waves, Appl. Opt. **43**, 2920 (2004).

[17] M. M. de Lima, Jr., M. Beck, R. Hey, and P. V. Santos, Compact Mach-Zehnder acousto-optic modulator, Appl. Phys. Lett. **89**, 121104 (2006).

[18] A. Crespo-Poveda, A. Hernández-Mínguez, B. Gargallo, K. Biermann, A. Tahraoui, P. V. Santos, P. Muñoz, A. Cantarero, M. M. de Lima, Jr., Acoustically driven arrayed waveguide grating, Opt. Express **23**, 21213 (2015)

[19] G. Bahl, J. Zehnpfennig, M. Tomes, and T. Carmon, Stimulated optomechanical excitation of surface acoustic waves in a microdevice, Nat. Commun. **2**, 403 (2011).

[20] K. C. Balram, M. I. Davanço, J. D. Song, and K. Srinivasan, Coherent coupling between radio frequency, optical, and acoustic waves in piezo-optomechanical circuits, Nat. Photonics **10**, 346 (2016).

[21] H. Li, S. A. Tadesse, Q. Liu, and M. Li, Nanophotonic cavity optomechanics with propagating acoustic waves at frequencies up to 12 GHz, Optica **2**, 826 (2015).

[22] M. M. de Lima, Jr., M. van der Poel, P. V. Santos, and J. M. Hvam, Phonon-Induced Polariton Superlattices, Phys. Rev. Lett. **97**, 045501 (2006).

[23] S. Kapfinger, T. Reichert, S. Lichtmannecker, K. Müller, J. J. Finley, A. Wixforth, M. Kaniber, and H. J. Krenner, Dynamic acousto-optic control of a strongly coupled photonic molecule, Nat. Commun. **6**, 8540 (2015).

[24] J. D. Thompson, B. M. Zwickl, A. M. Jayich, F. Marquardt, S. M. Girvin, and J. G. E. Harris, Strong dispersive coupling of a high-finesse cavity to a micromechanical membrane, Nature (London) **452**, 72 (2008).

[25] A. B. Matsko, A. A. Savchenkov, V. S. Ilchenko, D. Seidel, and L. Maleki, Optomechanics with Surface-Acoustic-Wave Whispering-Gallery Modes, Phys. Rev. Lett. **103**, 257403 (2009).

[26] V. S. Shumeiko, Quantum acousto-optic transducer for superconducting qubits, Phys. Rev. A **93**, 023838 (2016).

[27] V. Laude, C. F. Jerez-Hanckes, and S. Ballandras, Surface Green's function of a piezoelectric half-space, IEEE Trans. Ultrason. Ferroelectr. Freq. Control **53**, 420 (2006).

[28] V. Laude, D. Gérard, N. Khelfaoui, C. F. Jerez-Hanckes, S. Benchabane, and A. Khelif, Subwavelength focusing of surface acoustic waves generated by an annular interdigital transducer, Appl. Phys. Lett. **92**, 094104 (2008).

[29] J. Kushibiki, I. Takanaga, M. Arakawa, and T. Sannomiya, Accurate measurements of the acoustical physical constants of $LiNbO_3$ and $LiTaO_3$ single crystals, IEEE Trans. Ultrason. Ferroelectr. Freq. Control **46**, 1315 (1999).

[30] C. K. Campbell, *Surface Acoustic Wave Devices for Mobile and Wireless Communications* (Academic Press, San Diego, CA, 1998).

[31] K. Kokkonen and M. Kaivola, Scanning heterodyne laser interferometer for phase-sensitive absolute-amplitude measurements of surface vibrations, Appl. Phys. Lett. **92**, 063502 (2008).

[32] R. S. Weis and T. K. Gaylord, Lithium niobate: Summary of physical properties and crystal structure, Appl. Phys. A **37**, 191 (1985).

[33] M. Jazbinšek and M. Zgonik, Material tensor parameters of $LiNbO_3$ relevant for electro- and elasto-optics, Appl. Phys. B **74**, 407 (2002).

[34] R. W. P. Drever, J. L. Hall, F. V. Kowalski, J. Hough, G. M. Ford, A. J. Munley, and H. Ward, Laser phase and frequency stabilization using an optical resonator, Appl. Phys. B **31**, 97 (1983).

[35] D. Hunger, T. Steinmetz, Y. Colombe, C. Deutsch, T. W. Hänsch, and J. Reichel, A fiber Fabry-Perot cavity with high finesse, New J. Phys. **12**, 065038 (2010).

[36] N. E. Flowers-Jacobs, S. W. Hoch, J. C. Sankey, A. Kashkanova, A. M. Jayich, C. Deutsch, J. Reichel, and J. G. E. Harris, Fiber-cavity-based optomechanical device, Appl. Phys. Lett. **101**, 221109 (2012).